1976

Prediction of Heat and Mass Transfer During Compression in Reciprocating Compressors

M. S. Chong

H. C. Watson

PREDICTION OF HEAT AND MASS TRANSFER DURING COMPRESSION IN RECIPROCATING COMPRESSORS

M.S. Chong, Senior Research Assistant
H.C. Watson, Senior Lecturer
Department of Mechanical Engineering,
University of Melbourne, Parkville,
Victoria 3052, Australia

INTRODUCTION

In this paper we present an accurate procedure for predicting heat transfer and pressure variations in the cylinders of slow speed reciprocating air compressors. Currently, the influence of residual air motion at the end of the suction stroke is assumed to be small. Discharge of the compressed gas is also ignored.

The procedure has particular application to forecasting gas temperatures just prior to discharge including the spatial and temporal temperature variations within the cylinder. Thus surface heat fluxes can be calculated which can aid in the design of large compressors, or compressors made from thermally inferior materials such as plastics where heat transfer problems can lead to component failures.

MATHEMATICAL MODEL

The system considered is depicted in figure 1. The following assumptions are made:

- axisymmetric cylinder
- laminar flow
- specific heats vary with temperature alone.

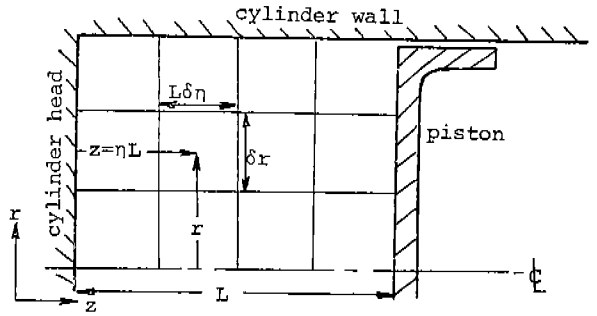

Figure 1. Schematic layout of compressor cylinder and piston

A cylindrical polar coordinate system is applied in which the number of grid nodes remains fixed. Thus the grid and individual control volumes contract as the piston moves towards the cylinder head.

The independent variables for the problem are the axial distance z, the radial distance r, and the time t. The dependent variables are the axial velocity u, the radial velocity v, the density ρ, the temperature T, and the pressure p.

For convenience, the axial coordinate is transformed by

$$z=\eta L \tag{1}$$

where η is the non-dimensional axial location of a cell, and L is the piston displacement.

Applying the transformation to the conservation equations (see ref. 1) for the system, we have:

Axial momentum conservation

$$\frac{\partial \rho u}{\partial t} + \frac{\rho u}{L}\frac{dL}{dt} + \frac{1}{L}\frac{\partial}{\partial \eta}\{\rho (u - \eta\frac{dL}{dt})u\} + \frac{1}{r}\frac{\partial (\rho uvr)}{\partial r}$$

$$= -\frac{1}{L}\frac{\partial p}{\partial \eta} + \mu\{\frac{1}{L^2}\frac{\partial^2 u}{\partial \eta^2} + \frac{1}{r}\frac{\partial}{r}(r\frac{\partial u}{r})\} \tag{2}$$

Radial momentum conservation

$$\frac{\partial \rho v}{\partial t} + \frac{\rho v}{L}\frac{dL}{dt} + \frac{1}{L}\frac{\partial}{\partial \eta}\{\rho (u - \eta\frac{dL}{dt})v\} + \frac{1}{r}\frac{\partial (\rho v^2 r)}{\partial r}$$

$$= -\frac{\partial p}{\partial r} + \mu\{\frac{1}{L^2}\frac{\partial^2 v}{\partial \eta^2} + \frac{1}{r}\frac{\partial}{\partial r}(r\frac{\partial v}{\partial r})\} \tag{3}$$

Mass conservation

$$\frac{\partial \rho}{\partial t} + \frac{\rho}{L}\frac{dL}{dt} + \frac{1}{L}\frac{\partial}{\partial \eta}\{\rho (u - \eta\frac{dL}{dt})\} + \frac{1}{r}\frac{\partial (\rho vr)}{\partial r} = 0 \tag{4}$$

Energy conservation

$$\frac{\partial \rho T}{\partial t} + \frac{\rho T}{L}\frac{dL}{dt} + \frac{1}{L}\frac{\partial}{\partial \eta}\{\rho(u - \eta\frac{dL}{dt})T\} + \frac{1}{r}\frac{\partial(\rho v T r)}{\partial r}$$

$$= \frac{\mu}{\sigma}\{\frac{1}{L^2}\frac{\partial^2 T}{\partial \eta^2} + \frac{1}{r}\frac{\partial}{\partial r}(r\frac{\partial T}{\partial r})\} + \frac{p}{c_p L}\frac{dL}{dt}^{*} \qquad (5)$$

FINITE DIFFERENCE EQUATIONS

Various numerical techniques using finite difference schemes can be used to approximate the above equations. The techniques employed here were obtained from a survey of relevant literature (ref. 2 to 9). Space limitations preclude the presentation of the finite difference equations, but the method is summarised as follows: the spatial variation of each variable is approximated using central differences and forward differences are used for the time derivatives. The non-linear terms are approximated using the backward or partial donor scheme.

SOLUTION PROCEDURE

The finite difference equations are solved in their primitive form (i.e. without the use of stream function and vorticity to simplify the equations). The procedure to solve the finite difference equations is outlined in the flow chart.

The numerical solution to this initial value problem is performed by means of a computer program run on a CDC 6400 machine. The computer time required to solve for the entire compression process is a function of the compression time, the size of the cylinder and the grid size. The time increment that is selected not only influences the number of integration steps required, but also the convergence stability which is in turn also affected by the geometry. It has been found expedient, in terms of improved computational efficiency, to vary the time increment with piston displacement. Computational time also increases in proportion to the increase in the number of cells in the cylinder.

Typically, computational time for a 5 by 10 cell system is about 200s for the 600 rev/min crank rotational speed tests discussed in the next section.

Provided the time increment is sufficiently small to maintain convergence, it has no influence on the computational precision; whereas, doubling the

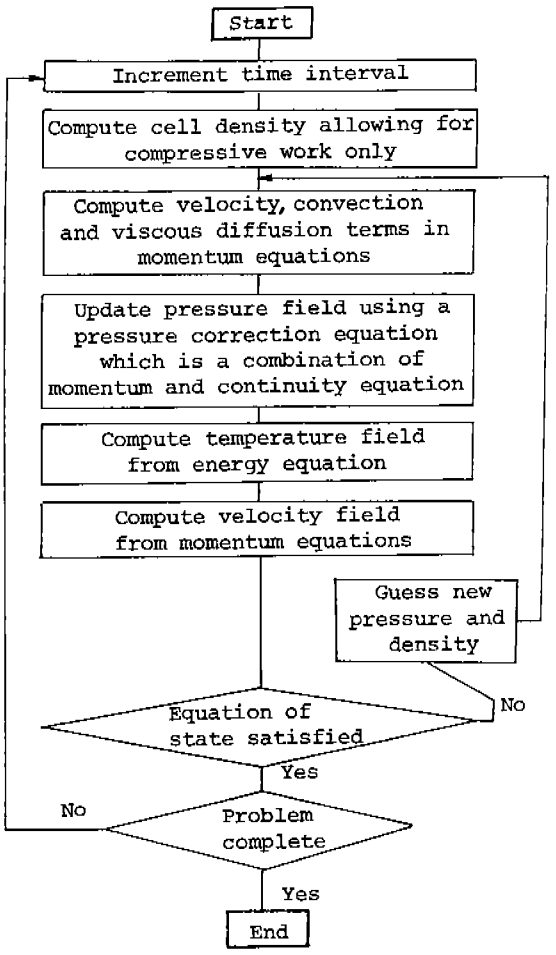

Flow Chart

number of cells can cause velocity changes of up to 15 percent. The increased computational accuracy in velocity estimation is offset by the increased computational time. Hence, ordinarily, 5 by 10 cell systems have been employed for the results now presented.

RESULTS

Predictionshave been made for the compression process of a compressor with a bore of 8.23 cm an a stroke of 12.7 cm. Results presented here are limited to two shaft speeds for which the flow field can be expected to be laminar (10 rev/min and 600 rev/min), at a compression ratio of 6:1 for atmospheric induction process and 373 K inducted gas temperature.

The results in figure 2 and 4 show temperatures, pressures, heat flux rates and velocities within the cylinder during the compression process.

For clarity of presentation, the velocity vectors in figures 2.3 and 4.3 are plotted on a non-

*In the derivation of the energy equation for fixed grid systems, the compression work term is assumed to be zero. For the above system where the cells are compressed, the work term can be obtained by assuming

$$W = \frac{dV}{dt}P$$

where W is the work done in compressing a cell and V is the volume of the cell.

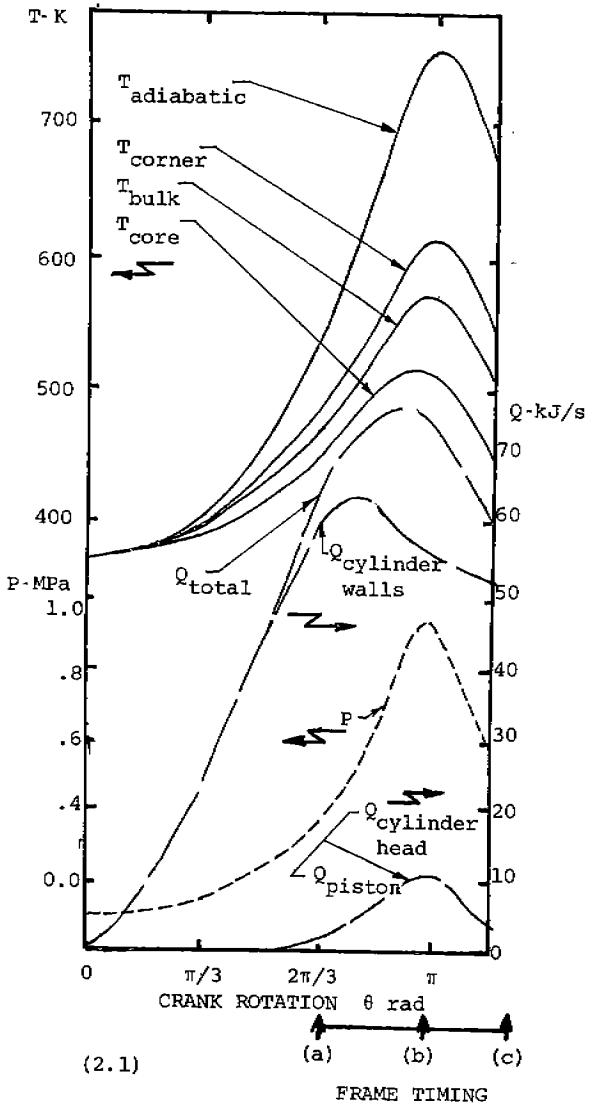

(2.1)

Figure 2. Predicted temperatures, pressures, heat flux rates and velocity vectors for compression of air at 10 rev/min rotational speed and 10:1 compression ratio.

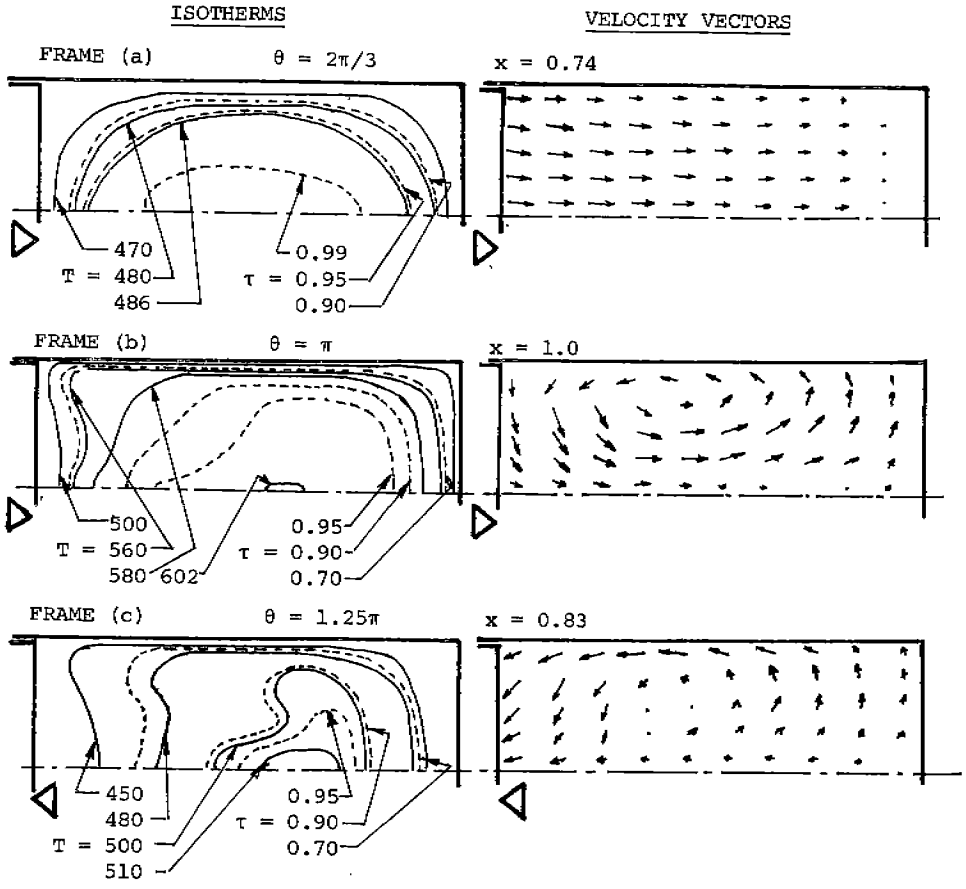

(2.2)

(2.3)

dimensional grid. The velocity vectors have been non-dimensionalised with respect to the maximum velocity existing within the flow field at each time increment. Thus comparison of the vectors in different frames will not represent the changes of magnitudes of the velocities over the time interval.

Examining first the slow speed results, we can see in figure 2.3, frame (a), that next to the cylinder walls a boundary layer, as depicted by the velocity variations with radius, has began to develop as the result of the velocity differential between the bulk fluid and that at the wall. By the end of the compression stroke, frame (b), a toroidal vortex has developed whose centre later, frame (c), moves towards the axis of the cylinder under the influence of the changed direction of action of the fluid shear forces near the cylinder walls, as the piston returns along the cylinder.

The effect of the fluid motion is to distort the isotherms shown in figure 2.2 from their regular shape. Also shown are contours of dimensionless temperature defference defined as

$$\tau = \frac{T - T_w}{\hat{T} - T_w} \qquad (6)$$

The formation of the vortex tends to increase heat transfer to the cylinder surfaces by forced convection. The central core of the hotter fluid is advected towards the colder wall regions of the cylinder head and walls, whilst the coldest fluid at the piston-crown cylinder-wall interface is forced towards the core, thus increasing the heat transfer over that due to conduction alone.

The effect of convection on the gas-wall heat transfer rates can be seen in figure 2.1. Heat transfer to each of the components, cylinder walls, cylinder head and piston crown is given here. All three are asymmetrical about the $\theta=\pi$ point with maxima accurring before this crank rotation,

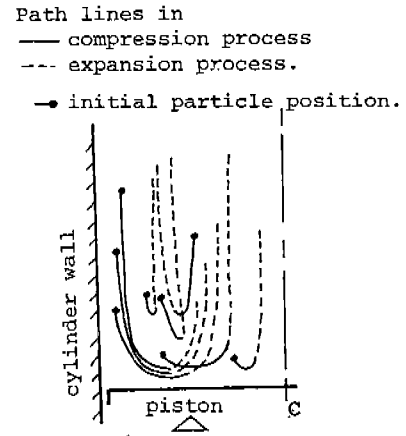

Figure 3. Path lines predicted for rotational speed of 10 rev/min and 6:1 compression ratio.

especially pronounced in the case of the gas-to-cylinder wall heat transfer. The peak of the heat flux to the cylinder walls is reached prior to maximum gas temperature because of the reducing area available fro heat transfer.

The continuous temporal description of the temperature of the gas in the piston-cylinder wall corner is given in figure 2.1, as are the core and spatially mean (bulk) temperature variations. Also shown is the bulk cylinder pressure variation. Spatial variations in pressure are small (less than 70 Pa) and therefore not presented.

In figure 3, the calculated movement of individual particles of air is traced as path lines. Because of the unsteady nature of the flow, the paths traced do not follow the velocity vectors, or the instantaneous stream-line patterns which can be obtained from figure 2.2, since the vectors change continuously in magnitude and direction with time. Thus, it can be seen that while most of the particle movement near the piston is in a radially inward direction, particles near the centre of the vortex move outwards as the centre shifts when the piston slows as θ approaches π.

The higher speed results, at 600 rev/min, but still the same compression ratio, are shown in figure 4. Whilst the general trends in velocity, temperature, pressure and heat fluxes are similar to those at the low speed, there are some notable differences in detail:

- Boundary layer growth is supressed at the higher speed and there is little if any recirculation of the fluid as can be seen in the velocity diagram in figure 4.3
- The thermal boundary layer, if defined by $\tau=.99$, extends to only about one twentieth of the bore diameter into the fluid at the higher speed, whereas at the low speed the whole of the fluid is influenced by the heat transfer process as may be seen by comparison of figures 4.2 with 2.2.
- The supression of convection at the higher speed results in almost symmetrical heat flux distributions to the cylinder surfaces about maximum piston travel at $\theta=\pi$ as can be observed in figure 4.1.
- Comparison of the pressure development in figure 2.1 and 4.1 shows that predicted peak pressure is about 7 percent higher at the faster speed despite the increase in peak total heat flux of 30 percent.

Also shown in figure 4.1 are experimentally observed cylinder pressures in a motored reciprocating engine from earlier research by the authors (ref. 10, 11). The error in pressure prediction for three compression ratios is summarised in figure 5 where the error Δp is defined as

$$\Delta p = \frac{p_{predicted} - p_{measured}}{p_{max,measured}} \qquad (7)$$

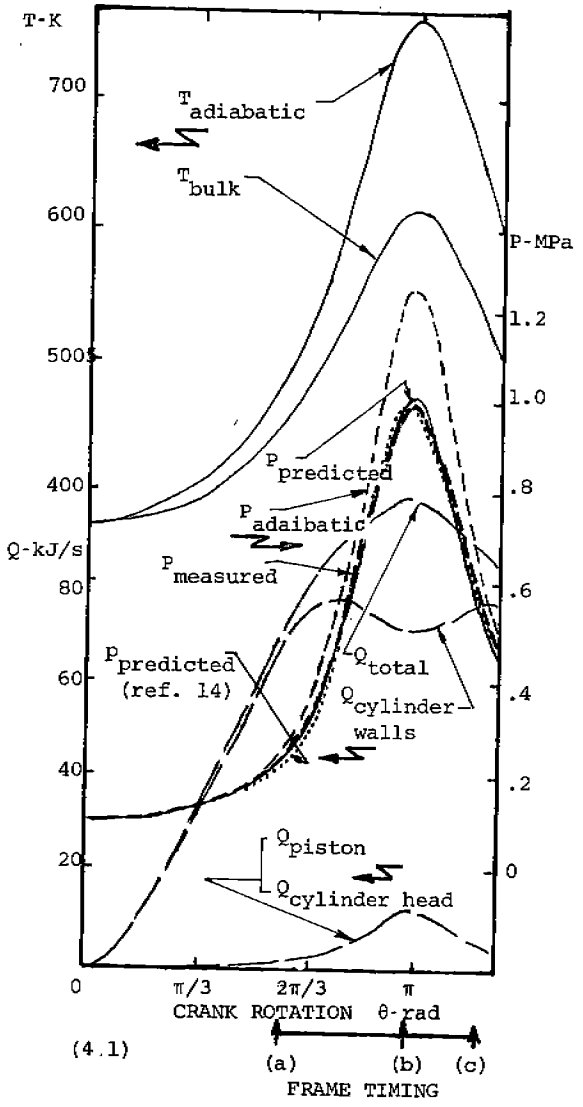

Figure 4. Predicted temperatures, pressures, heat flux rates and velocity vectors, and measured pressure for compression of air at 600 rev/min rotational speed and 6:1 compression ratio.

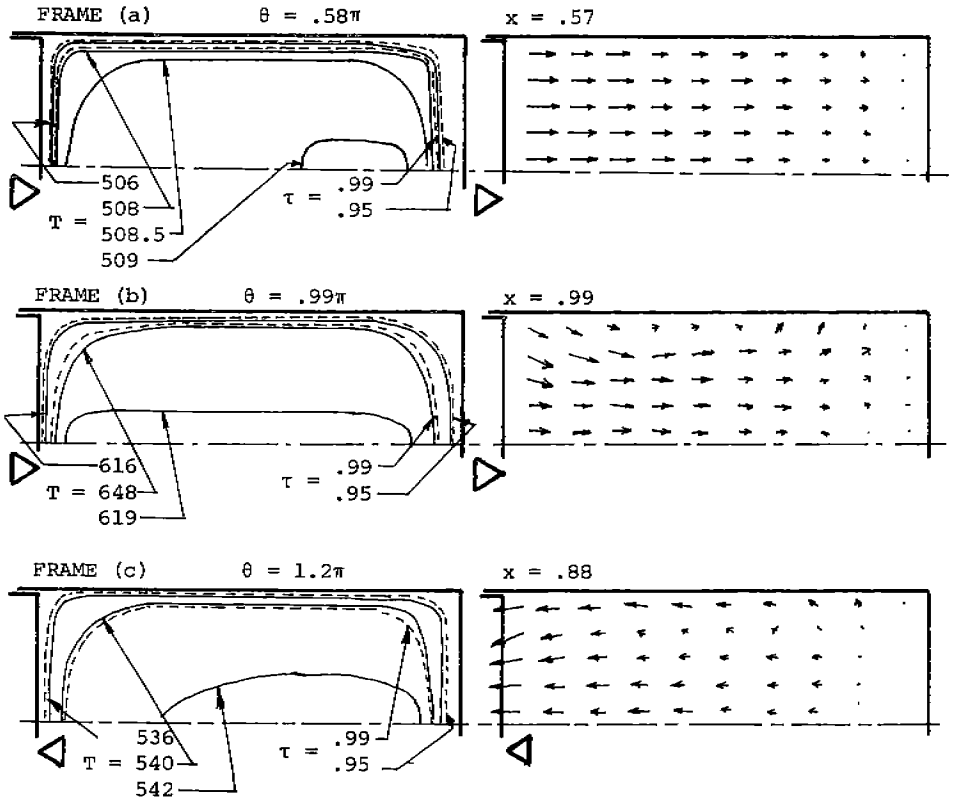

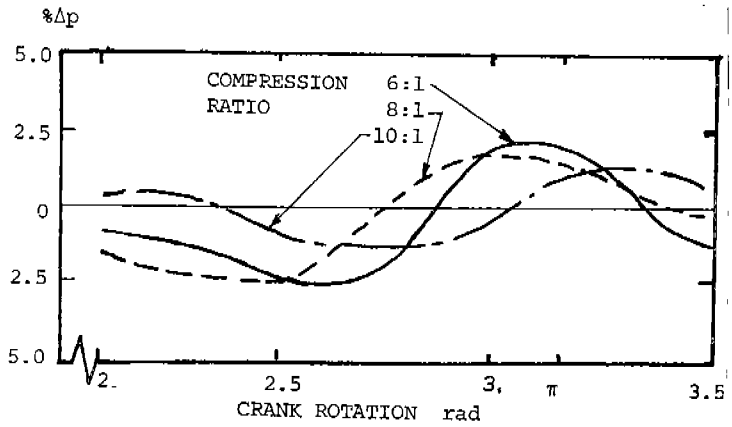

Figure 5. Pressure error %Δp versus crank rotation at 600 rev/min rotational speed for 3 compression ratios.

It is clear that the experimental results are predicted within ±2 percent with an average error of 1.2 percent. This compares very favourably with the expected experimental error in pressure measurement of 1.1 percent in engine cylinders (ref. 12).

DISCUSSION

It has been shown that as the compressor rotational speed changes between 10 and 600 rev/min, convection is supressed. Runs at intermediate speeds show that the convective component of heat transfer is not significant beyond about 100 rev/min.

This finding implies that at speeds greater than 100 rev/min, for the size of cylinder currently considered, the need to solve the combined momentum, mass, state and energy conservation equations is removed. Heat transfer, as a term of the energy equation for the whole in-cylinder system can be considered as a conduction only problem, and because of the proven thinness of the thermal boundary layer, the problem may be treated as one dimensional for each of the cylinder, cylinder head and piston surfaces.

The one dimensional conductive heat approach has been applied to reciprocating compressor heat transfer by Wendland (ref 13) and to reciprocating engines by Hii (ref. 14). Hii's results have been added to figure 4.1. Here we have provided the substantive evidence for this approach.

We anticipate that at high speeds,* as the Reynolds number for in-cylinder flow increases, that the boundary layer along the cylinder wall may become turbulent and the need could arise to replace the thermal conductivity by an effective conductivity or to return to the combined equations.

It is our intention to investigate the influence of turbulence by the addition of a simple turbulence model to the equations given above. We also hope to consider the influence of inlet valve induced swirl on heat and mass transfer.

*At 600 rev/min rotational speed, the Reynolds number is 7,000.

CONCLUSION

The non-steady equations for conservation of momentum, mass, energy and state have been solved by numerical methods for the fluid contained in the axi-symmetric cylinder of a reciprocating compressor. Both heat and mass transfer have been predicted during the compression process and the pressure development has been shown to be in close agreement (±2 percent) with experimental measurements.

It has been shown that at low crank shaft rotational speeds, i.e 10 rev/min, there is significant mass transport due to a toroidal vortex motion induced in the cylinder by the motion of the piston. As speeds increase, this motion is supressed and heat transfer by conduction alone becomes dominant as the thermal boundary layer reduces. The boundary layer thickness is one twentieth of the cylinder bore diameter at the end of compression at 600 rev/min for the size of cylinder considered. Under these conditions it is proposed that the analysis of the system may be simplified and the system considered as spatially uniform with one dimensional heat transfer at all the cylinder surfaces.

LIST OF SYMBOLS

c_p	specific heat at constant pressure
L	piston displacement from cylinder head
p	cylinder pressure
Δp	$(p_{predicted} - p_{measured})/p_{max,measured}$
Q	heat flux rate
r	radial distance from cylinder axis
T	temperature
T_w	wall temperature
$\hat{T}$	maximum temperature
u	axial velocity
v	radial velocity
x	$(L_{max} - L)/(L_{max} - L_{min})$
z	axial distance from cylinder head
η	z/L
θ	crank rotation
μ	fluid viscosity
ρ	fluid density
σ	Prandtl number
τ	$(T - T_w)/(\hat{T} - T_w)$

REFERENCES

1. Chong, M.S., "Numerical simulation of air motion within the cylinder of a reciprocating engine," Ph.D Thesis, University of Melbourne, 1976.

2. Amsden, A.A. & Harlow, F.H., "The SMAC method: a numerical technique for calculating incompressible fluid flows," Los Alamos Scientific Laboratory Report LA-4370, 1970.

3. Caretto, L.S., Gosman, A.D. Patankar, S.V., & Spalding, D.B., "Two calculation procedure for steady, three-dimensional flows with circulation," Imperial College, London, Technical Report EF/TN/A/47, 1972.

4. Chorin, A.J. "Numerical solution of Navier-Stokes equation," Math. Comp. Vol.22, 1968.

5. Gosman, A.D., Pun, W.M., Runchal, A.K., Spalding, D.B. & Wolfstein, M., "Heat and mass transfer in recirculating flow," Academic Press, 1969.

6. Harlow, F.H. & Welch, J.E., "Numerical calculation of time-dependent incompressible flow," The Phys. of Fluids Vol.8, 1965.

7. Patankar, S.V. & Spalding, D.B., "Numerical prediction of three dimensional flows," Imperial College, London, Technical Report EF/TN/A/46, 1972.

8. Viecelli, J.A., "A computing method for the incompressible flow bounded by moving walls," Jnl. Comp. Physics, Vol.8, No.1, 1971.

9. Young, J.A. & Hirt, C.W., "Numerical calculation of internal wave motion," Jnl. Fluid Mechanics, Vol. 56, Pt.2, 1972.

10. Chong, M.S., "Heat transfer in motored engines," M.Eng.Sc Thesis, University of Melbourne, 1971.

11. Edwards, M. & Fillingham, G., "Heat transfer in motored engines," Unpublished special project report, University of Melbourne, 1974.

12. Watson, H.C., "Compression ignition of fuel oxidant mixtures," Imperial College, London, Mech. Eng. Dept. Report CCK/R1, 1970.

13. Wendland, D.W., "The effect of periodic pressure and temperature fluctuations on unsteady heat transfer in a closed system," NASA Report CA-72323, 1968.

14. Hii, S., "Simulation of the residual gas ignition of hydrogen," M.Eng. Sc Thesis, University of Melbourne, 1976.